RESEARCH ARTICLE
PLANETARY SCIENCE

*Earth and Planetary Physics*
*2*: 15–21, 2018
doi: 10.26464/epp2018002

# First results of optical meteor and meteor trail irregularity from simultaneous Sanya radar and video observations

**GuoZhu Li[1,2,3,4*], BaiQi Ning[1,2,3,4], Ao Li[1,4], SiPeng Yang[3], XiuKuan Zhao[3], BiQiang Zhao[1,2,3,4], and WeiXing Wan[1,2,3,4]**

[1]Key Laboratory of Earth and Planetary Physics, Institute of Geology and Geophysics, Chinese Academy of Sciences, Beijing 100029, China;

[2]Institutions of Earth Science, Chinese Academy of Sciences, Beijing 100029, China;

[3]Beijing National Observatory of Space Environment, Institute of Geology and Geophysics, Chinese Academy of Sciences, Beijing 100029, China;

[4]University of Chinese Academy of Sciences, Beijing 100049, China

**Abstract:** Meteoroids entering the Earth's atmosphere can create meteor trail irregularity seriously disturbing the background ionosphere. Although numerous observations of meteor trail irregularities were performed with VHF/UHF coherent scatter radars in the past, no simultaneous radar and optical instruments were employed to investigate the characteristics of meteor trail irregularity and its corresponding meteoroid. By installing multiple video cameras near the Sanya VHF radar site, an observational campaign was conducted during the period from November 2016 to February 2017. A total of 242 optical meteors with simultaneous non-specular echoes backscattered from the plasma irregularities generated in the corresponding meteor trails were identified. A good agreement between the angular positions of non-specular echoes derived from the Sanya radar interferometer and those of optical meteors was found, validating that the radar system phase offsets have been properly calibrated. The results also verify the interferometry capability of Sanya radar for meteor trail irregularity observation. The non-specular echoes with simultaneous optical meteors were detected at magnetic aspect angles greater than ~78°. Based on the meteor visual magnitude estimated from the optical data, it was found that the radar non-specular echoes corresponding to brighter meteors survived for longer duration. This could provide observational evidence for the significance of meteoroid mass on the duration of meteor trail irregularity. On the other hand, the simultaneous radar and video common-volume observations showed that there were some cases with optical meteors but without radar non-specular echoes. One possibility could be that some of the optical meteors appeared at extremely low altitudes where meteor trail irregularities rarely occur.

**Keywords:** meteor; ionosphere; radar; non-specular echo

**Citation:** Li, G. Z., Ning, B. Q., Li, A., Yang, S. P., Zhao, X. K., Zhao, B. Q., and Wan, W. X. (2018). First results of optical meteor and meteor trail irregularity from simultaneous Sanya radar and video observations. *Earth Planet. Phys.*, *2*, 15–21. http://doi.org/10.26464/epp2018002

## 1. Introduction

Every day, billions of meteoroids, which have typical sizes ranging from 0.05 mm to 20 cm, enter the Earth's atmosphere and give rise to several phenomena: (1) creating meteor light through the radiation of excited atoms from meteoroid material vapors that can be detected by optical instrument, (2) changing the ionospheric composition especially during meteor shower, with evidence from rocket in-situ measurements by ion mass spectrometer, and (3) producing numerous ionized columns followed by development of meteor plasma density irregularity that are also known as radar meteor trails with "ridges and troughs", significantly disturbing the background ionosphere and scattering radio waves (e.g., Mathews et al., 1997; Ceplecha et al., 1998; Oppenheim and Dimant, 2006; Dou XK et al., 2010).

Radar observations of meteor plasma density have shown three types of echoes including head echo, specular echo and non-specular echo. The head echo, mainly detected by High Power Large Aperture (HPLA) radars with peak powers of several hundred kilo-watt to several mega-watt, is due to the scattering of meteor plasma surrounding meteoroid during its atmospheric flight. Specular and non-specular echoes, both scattered from plasma in meteor trail, can be simultaneously detected (e.g., Chau et al., 2014), and be utilized as tracers to derive lower thermosphere wind (e.g., Oppenheim et al., 2009; Li GZ et al., 2012; Reid, 2015). For specular echo, it usually appears at one range gate with short duration of less than 1 second, being observed when radar line-of-sight (LOS) is perpendicular to meteor trail. Non-specular echo, also known as range spread trail echo, covers a few range gates and can survive for a long time up to minutes (e.g., Li GZ et al., 2014a, and references therein). Theoretical simulations showed that non-specular echo could result from Bragg scattering from plasma irregularities generated in meteor trail through the two-stream (Farley-Buneman) or gradient-drift instabilities driven by wind/electric fields (e.g., Chapin and Kudeki, 1994; Oppenheim and Dimant, 2015). By employing the interferometry capability of HPLA radars, for example the MU (Middle and Upper atmosphere) and ALTAIR radars, non-specular echoes were found to be mostly from the region where radar LOS is perpendicular to

Correspondence to: G. Z. Li, gzlee@mail.iggcas.ac.cn
Received 21 OCT 2017; Accepted 05 NOV 2017.
Accepted article online 04 DEC 2017.

the geomagnetic field ***B*** (e.g., Zhou QH et al., 2001), with a cutting magnetic aspect angle (between radar line-of-sight and geomagnetic field) of ~78° (Close et al., 2008). However, a recent study from the Middle Atmosphere Alomar Radar System (MAARSY) reported several cases of long-duration non-specular echoes coming from the region where radar LOS is nearly parallel to ***B***, indicating that the magnetic aspect angles get down to around 0° (Chau et al., 2014).

For non-specular echoes surviving for a long time up to tens of seconds (e.g., Chu YH and Wang CY, 2003), even up to 30 minutes observed by ionosonde (Maruyama et al., 2008), the generation mechanisms are not well understood. Based on the change in the non-specular echo Doppler velocity at different range bins, a large wind shear was suggested to be a possible candidate to account for the long duration of non-specular echo (e.g., Bourdillon et al., 2005). Considering the fact that both long and short duration non-specular echoes were near simultaneously detected in a limited area during a short time interval when the background neutral wind did not vary much (e.g., Li GZ et al., 2012, 2014a), the wind shear seems unlikely to be the only factor determining the duration of non-specular echo. Theoretical studies showed that the mass and composition of meteoroid creating meteor trail irregularity are important factors controlling the duration of non-specular echo (e.g., Kelley, 2004; Dyrud et al., 2007; Chau et al., 2014). On the other hand, a statistical analysis on the correlation between non-specular echo duration and magnetic aspect angle showed that the majority of long duration non-specular echoes come from the region where radar LOS is perpendicular to ***B*** (Close et al., 2008). It was suggested that the "radio science perspective" of non-specular echoes, i.e., the angle between radar LOS and the direction perpendicular to ***B*** could also affect the duration (Malhotra et al., 2007).

To understand the factors controlling the generation and development of meteor trail irregularity and the features of meteoroid producing the trail, we conducted an observational campaign at Sanya during November 2016–February 2017 by employing the Sanya VHF radar interferometer together with the optical system consisting of seven video cameras newly installed near the radar site. Although there have been many observational studies of non-specular echoes created by meteor trail irregularities by using radar and meteoroids using optical instruments, there is a lack of studies that combine radar observations of non-specular echoes with simultaneous optical signatures of meteor trails, to reveal the link between the characteristics of non-specular echoes and meteoroids. On the other hand, for radar interferometry observations of non-specular echoes, an important prerequisite is the calibration of radar system phase offsets, and elimination of angular ambiguity considering that the non-specular echo in radar side-lobes might also be detected, especially for HPLA radars. Because of the small power of the Sanya radar, our previous work did not consider the possible side-lobe effect, when the radar system phase offsets were self-calibrated by using E region field-aligned irregularity (FAI) echo. Based on simultaneous optical meteor and radar non-specular echo observations, further verification of the Sanya radar interferometry capability which was expected to shed light on the generation and evolution of meteor trail irregularity is also the focus of the present study.

## 2. Experimental Details

The Sanya VHF radar, with an operational frequency of 47.5 MHz and a peak power of 24 kW, has been operated since February 2009. The radar antenna array consists of 24 Yagi antennas, which were grouped into 6 modules (each module consisting of 2×2 Yagi antennas) aligned in the east-west direction for transmission and reception. This main antenna array has been widely utilized to investigate the statistical occurrence characteristics of ionospheric irregularity, e.g., sporadic-E and spread-F irregularities over Sanya (e.g., Ning BQ et al., 2012; Li GZ et al., 2011, 2015, 2016). To get the positions of irregularity scatters in the Sanya radar illuminated region, especially for the irregularities with weak magnetic aspect sensitivity, we upgraded the Sanya radar system by installing a new module (2×2 Yagi antennas) only for reception in the north of the main east-west antenna array in December 2012 (Li GZ et al., 2014b). By using any two modules of the east-west antenna array, together with the newly added north module, the position of irregularity scatters can be estimated through spatial domain interferometry. For the observations presented here, the Sanya radar interferometer setup and radar experimental parameters were similar to those used for non-specular echo observation in July–August 2013 (Li GZ et al., 2014a, c). In brief, the pulse repetition frequency, pulse length, range resolution and sampled range interval are 650 Hz, 6 μs, 0.9 km, and 80–200.6 km, respectively. All of the raw complex (I/Q components) data were recorded for off-line interferometry analysis.

For video observation of meteors, we used 7–33 mm f/0.95 Hikvision lens (auto iris used to reduce the possibility of pixel saturation) coupled to low-lux Watec 902H2 ultimate CCD video cameras, and digitized the video with Canopus A/D converters to disk through PCI-1394 frame-grabber cards. The digitized video images with 720×576 pixel resolution (8-bits depth) were stored on disk in AVI format (no compression involved), at a rate of 25 frames per second. In order to improve the sensitivity for observing faint meteors and achieve a field-of-view (FOV) similar to that of the Sanya radar main beam, a total of seven video cameras were installed near the Sanya radar site, where each camera was operated with a relatively small FOV of about 12°×15° and pointed around the center of the Sanya radar main beam. This optical system provides an angular resolution of about 0.02° per pixel with a limited stellar magnitude of about +6. The FOV of Sanya radar 3-dB full beam (transmission) and the optical system (including seven video cameras) are shown in Figure 1, as functions of azimuth and zenith (in degree).

## 3. Methodology

During the period from November 2016 to February 2017, a total of 60 nights of simultaneous radar and video data were recorded. By employing radar interferometry technique, the angular position of non-specular echo produced by meteor trail irregularity can be estimated from the multi-channel raw complex data. Based on the pixel intensity and angular position (azimuth and zenith) of background stars from the video data, the visual magnitude and angular position of optical meteor can be calculated by using the

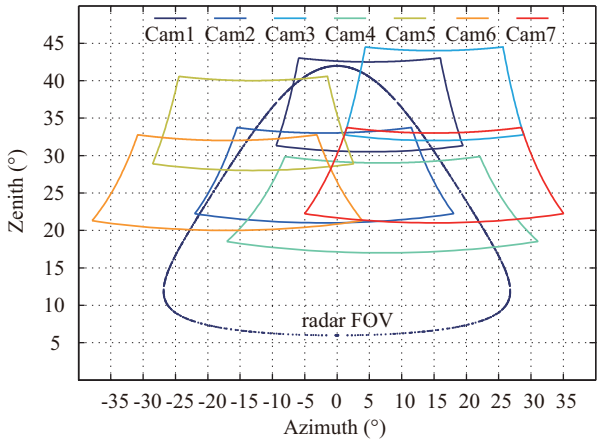


**Figure 1**. FOV of the Sanya VHF radar (3-dB full beam width) and optical system (consisting of seven video cameras) as functions of azimuth and zenith in degrees.

standard routines for meteor photometry.

### 3.1 Radar Interferometry

For the Sanya VHF radar interferometer employed for the observation of meteor trail irregularity during the present experiment, a total of six channels (five in the east-west, and one in north) were used for reception. By using the complex output from any two channels in the east-west and north channel, for example the channels marked as '2', '3' and '7' (see also Figure 1 of Li GZ et al., 2014b), the angular position (azimuth and zenith angles, $\varphi$ and $\theta$) of irregularity scatters can be calculated using the following equations,

$$\varphi = \cot^{-1}\left[\frac{d_{23}(\Delta\Phi_{37} + \Phi_{\text{bias37}} + 2\pi l)}{d_{37}(\Delta\Phi_{23} + \Phi_{\text{bias23}} + 2\pi m)}\right]$$

and

$$\theta = \cos^{-1}\left[\frac{(\Delta\Phi_{23} + \Phi_{\text{bias23}} + 2\pi m)}{k d_{23}\sin(\phi)}\right],$$

where $d_{23}$ and $d_{37}$, $\Phi_{\text{bias23}}$ and $\Phi_{\text{bias37}}$ are the separations, and radar system phase offsets between the channels, respectively. $l$ and $m$ are the interferometry lobe numbers (multiples of 2π). $\Delta\Phi_{23}$ and $\Delta\Phi_{37}$ are the phase differences calculated by using the complex output from the three channels. The calculation of $\Delta\Phi$, $\Phi_{\text{bias}}$, $l$ and $m$ was detailed in our previous work (e.g., Li GZ et al., 2014b) and will not be repeated here.

### 3.2 Meteor Photometry

For meteor observation by the optical system, first the angular position of image pixel was calculated by employing the positions of background stars detected in the FOV of the cameras. Then the angular position of meteor was obtained. By following a method similar to that used in Hawkes et al. (2001) and Kikwaya et al. (2010), the apparent visual magnitude of meteor (frame by frame) was obtained through calibrating the log-sum-pixel of meteor with those of the observed stars (calibration was performed separately for each meteor event). For the calculation of log-sum-pixel of the star, the pixels from the area of a circular disc covering the whole star and the pixels taken from a ring surrounding the star that represent the background value were used. The catalogue SKY 2000v4 (Myers et al., 2001) was employed in the calibration.

Figure 2 shows an example of a meteor observed on 17 December 2016 at 19:33 UT (LT=UT+7.6 h) by the camera number 6. The meteor image, calculated angular position, photometric calibration and measured light curve (apparent visual magnitude) are shown in panels a, b, c and d, respectively. This meteor was found initially appearing at the angular position −12°/27° (azimuth/zenith) and disappearing at −31°/32° (Figure 2b), with a maximum visual magnitude of about −1.3. For statistical analysis on the correlation between non-specular echo duration and meteor visual magnitude, only the maximum value of visual magnitude (for each meteor) will be used.

## 4. Results and Discussion

Figure 3 shows three cases of meteors simultaneously observed by the Sanya radar (range-time-intensity plots) and optical system (images) at 21:41 UT on 19 November 2016, 18:46 UT on 25 December 2016, and 19:24 UT on 28 January 2017, respectively. The three meteors (numbered 1–3 from left to right) had maximum visual magnitudes of about −1.4, 0.8, and 3.2, respectively (top panels). For the brighter meteors #1 and #2, the corresponding non-specular echoes scattered from the irregularities generated in the meteor trails continued for more than 30 s with signal-to-noise ratio (SNR) >0 dB, both belonging to the long-duration echo type defined by Malhotra et al. (2007) and Sugar et al. (2010). The echoing shapes, however, show different features in the radar range-time-intensity plots. It can be seen from the bottom panels of Figure 3 that the non-specular echoes of meteor #1 had an initial triangular shape with the lower part continuing for a long time. For the meteor #2, the non-specular echo intensity during the initial several seconds was very strong at nearly all range gates around 115–125 km, and then the echoes at upper and lower range gates disappeared abruptly. For the faint meteor #3, the non-specular echoes only existed for a short duration of less than 5 s.

The angular positions of these meteors can be derived from both the optical and radar data by employing the methods mentioned above. Figure 4 shows the angular locations of optical meteors and of radar non-specular echoes for the three cases. The empty circles represent the locations of non-specular echoes derived from the radar interferometry, with different colors marking the altitudes. The solid curve shows the angular location of optical meteor. The shaded area represents the directions where the Sanya radar LOS is perpendicular to $\boldsymbol{B}$ at altitudes of 90–130 km. It can be clearly seen from Figure 4 that the angular locations of radar non-specular echoes and optical meteors, in general, correspond well, except the spread in the positions of non-specular echoes (derived from the Sanya radar). This spread could be easily understood because previous theoretical simulations have shown that after the passage of a meteor, the plasma column that it leaves behind will expand rapidly and develop turbulence forming highly structured plasma irregularity, which can extend along $\boldsymbol{B}$ for a long distance being detected by radar (e.g. Oppenheim and Dimant, 2015). The good agreement between the angular loca-

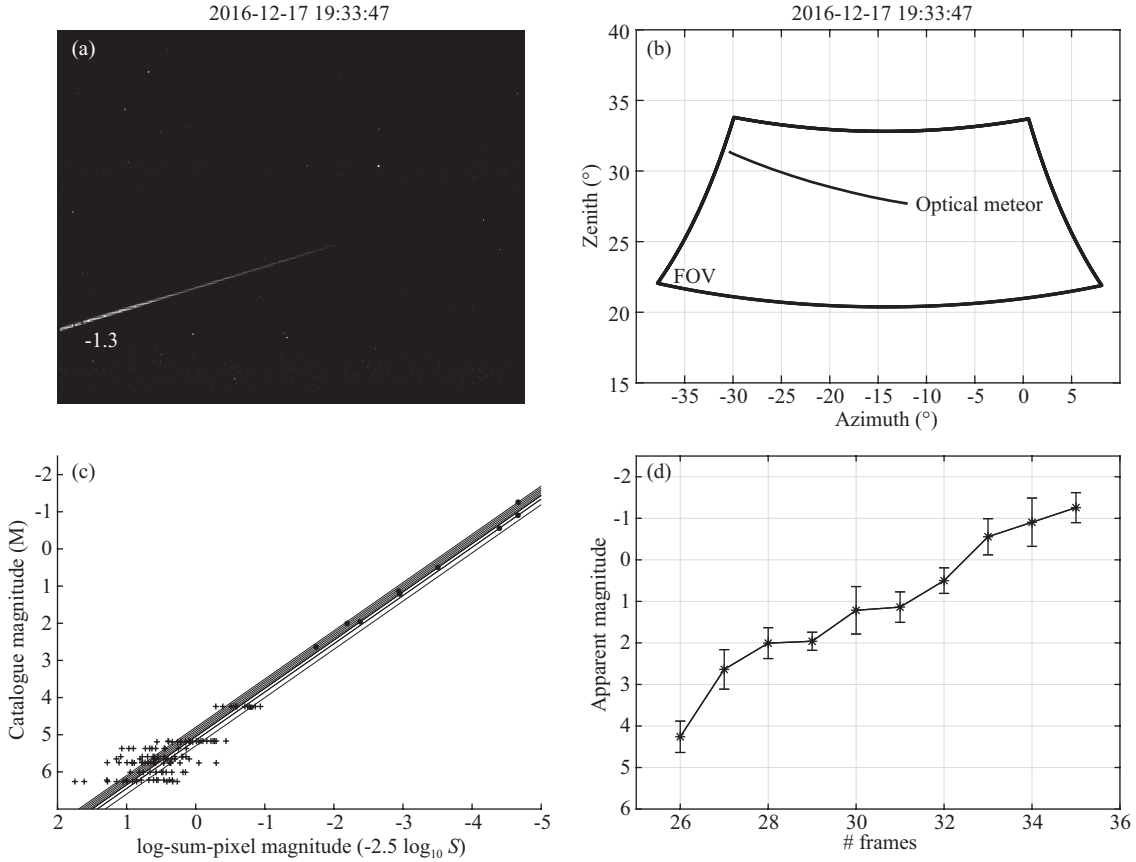


**Figure 2**. An example of a meteor observed on 17 December 2016 at 19:33 UT. (a) Meteor image, (b) angular location of the optical meteor as functions of azimuth and zenith in degrees, (c) photometric calibration between the catalogue SKY 2000v4 magnitude and log-sum-pixel value ($-2.5\log_{10}S$, where $S$ is the background subtracted intensity sum of Star/Meteor), and (d) measured light curve. For this case, the maximum visual magnitude could be biased because only part of the meteor was detected due to the limited FOV.

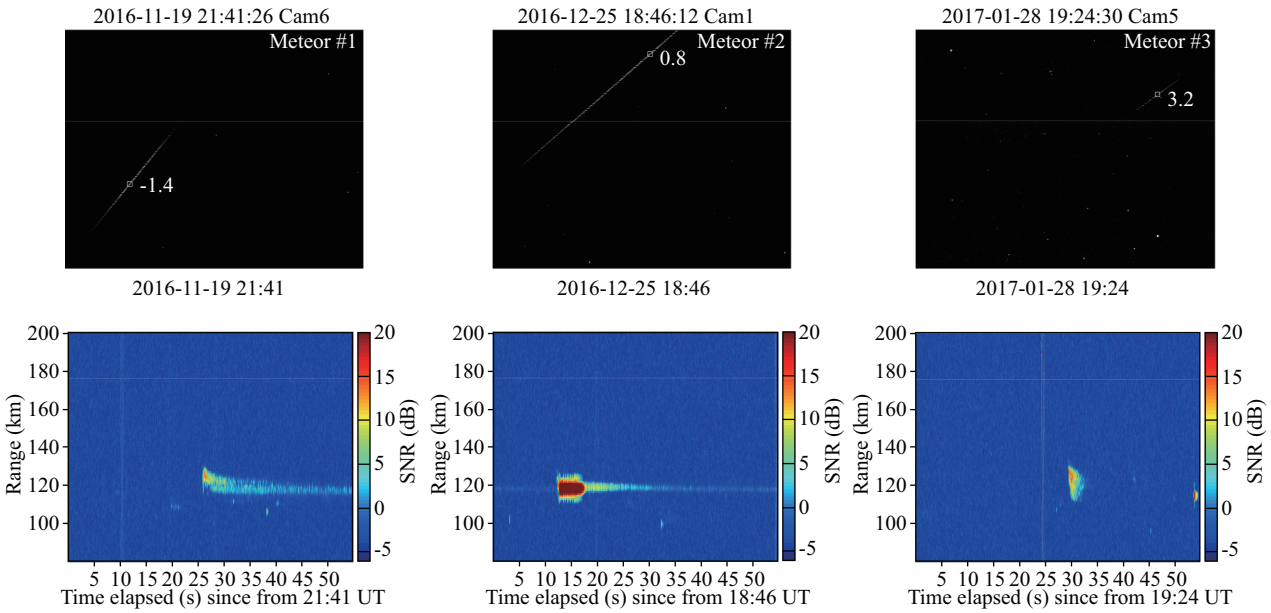


**Figure 3**. (top) The meteor images and (bottom) corresponding radar returns from irregularities generated in meteor trail simultaneously observed by the optical system and radar for three meteors at 21:41 UT on 19 November 2016 (Cam6), 18:46 on 25 December 2016 (Cam1) and 19:24 on 28 January 2017 (Cam5), respectively. The maximum visual magnitude is shown in each image.

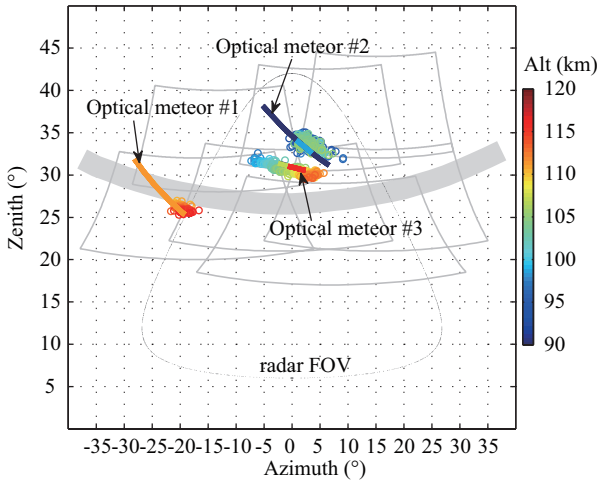


**Figure 4**. The angular locations of optical meteors (solid lines) and non-specular meteor echoes (circles with different colors representing the altitudes) derived from the radar interferometry for the three cases shown in Figure 3. The shaded area represents the directions where the Sanya radar LOS is perpendicular to ***B*** at the altitude interval 90–130 km.

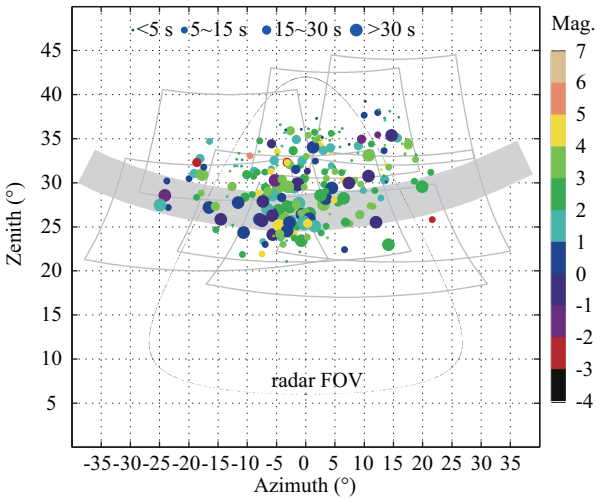


**Figure 5**. The angular locations of meteors observed by the Sanya radar and optical system during the period from November 2016 to February 2017 (a total of 242 events). For each dot, the color and size represent the maximum visual magnitude and duration, respectively.

tions suggests that these meteors simultaneously detected by the radar and optical instruments are the same events, and also verifies the interferometry capability of Sanya radar for meteor trail irregularity observation. Another feature seen in Figure 4 is that the non-specular echoes were not always observed in the whole path of optical meteor, even at altitudes around 100 km where plasma irregularities are usually thought to be easily generated in meteor trail. For the faint meteor #3, its corresponding non-specular echoes appeared in the whole path of optical meteor. However, for the meteors #1 and #2, the non-specular echoes were detected only in portions of the optical meteor paths. Due to the fact that meteor plasma (and its associated irregularity) should have been generated along the whole path of optical meteor which appeared in the altitudes range of 90–120 km, the absence of non-specular echo could indicate that the echo intensity scattered from the meteor trail irregularities generated in the region away from the radar main beam (meteor #1) or away from perpendicular to ***B*** (meteor #2) was significantly reduced below the detection limit of Sanya radar.

During the period from November 2016 to February 2017, there are a total of 242 meteor events in which good agreements between the positions of simultaneous radar non-specular echoes and optical meteors were found. Figure 5 shows the angular positions of all the meteor events. For each meteor, only the central position derived from the radar data is used, and shown as dot in the Figure. The color and size of the dot represent the maximum visual magnitude and duration of non-specular echoes, respectively. Two notable features can be seen in this Figure. One is that most of these meteors were detected in the radar main beam. In general, the positions of meteors were not far from the directions where radar LOS is perpendicular to ***B*** (as indicated by the shaded area in Figure 5). For these meteor events, the maximum angle between radar LOS where non-specular echoes were observed and the direction perpendicular to ***B***, is about 12° (for example, the direction with azimuth and zenith angles of 10° and 40°, where non-specular echo was observed, is about 12° away from the direction perpendicular to ***B***). This is consistent with the Kwajalein HPLA radar observations showing the cutoff angle of 12° for radar trail detection (Close et al., 2008). On the other hand, both the non-specular echoes associated with faint meteors and long-duration (>30 s) non-specular echoes were detected at directions far away from perpendicular to ***B***, indicating that the meteor trail irregularities producing long duration non-specular echoes are not exclusively situated in the region perpendicular to ***B***.

Figure 6 shows the maximum visual magnitudes plotted against the durations of corresponding non-specular echoes. To reduce the possible effect of "radio science perspective" on the duration,

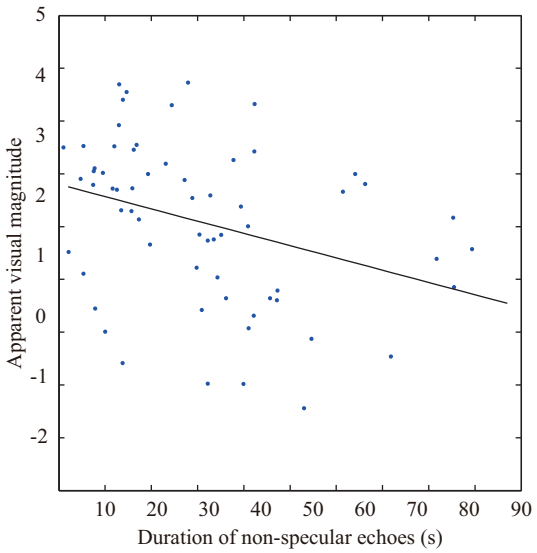


**Figure 6**. Plot of non-specular echo duration versus maximum visual magnitude for the meteor events appeared in the directions where the radar LOS is not far from perpendicular to ***B*** (90±2°).

only the meteors appeared in the directions where the radar LOS is not far from perpendicular to $\boldsymbol{B}$ (90±2°) were considered. A general linear relationship exists between the non-specular echo duration and its corresponding meteor visual magnitude. Due to lack of meteor velocity which is necessary for estimating the mass of meteoroid lost in the portion of the optical meteor, a definitive relationship between the meteor mass and non-specular echo duration cannot be obtained from the present single site observation. Based on the relation of meteor mass ($m$) and related parameters, that is

$$P_{0M}10^{-0.4M} = \tau\frac{1}{2}\frac{\mathrm{d}m}{\mathrm{d}t}v^2$$

(e.g., Campbell-Brown et al., 2012) (where $P_{0M}$, $M$, $\tau$, $v$ are the power of the photons observed by the optical instrument from a magnitude 0 star, meteor visual magnitude, luminous efficiency, and velocity during a time interval d$t$, respectively), the present initial result could support earlier theoretical simulations that the meteors with large (for example milligram) and small (for example microgram) mass potentially produce long and short duration non-specular echoes, respectively (Dyrud et al., 2007). To quantify the relationship between meteor mass and non-specular echo duration, we are planning to perform further experiments by using double-station video observations, together with the Sanya VHF radar in the near future.

Besides the cases of meteors (named type-I) simultaneously detected by the radar and optical system in the same angular location, there are the other two types of events: One (type-II) is that meteors were near simultaneously detected by both systems but not in the same angular location (possibly not the same meteor event). The other (type-III) is that optical meteors were detected but without simultaneous radar non-specular echoes. Figure 7 shows the angular locations of type-III meteors. The majority of these optical events were observed outside the FOV of radar main beam. For these optical meteors, there are several possibilities that could cause the absence of corresponding non-specular echoes. One is that meteor trail irregularities were generated, but the echo intensity scattered from the irregularities was below the detection limit of the radar. Using the ALTAIR radar observations, Close et al. (2008) found that the intensities of non-specular echoes decrease at a rate of about 3±2 dB/degree when the radar points away from the direction perpendicular to $\boldsymbol{B}$. For some of the faint meteors appeared far away from the radar main beam and/or from the direction perpendicular to $\boldsymbol{B}$, the echo intensity scattered from the trail irregularities could be significantly reduced below the detection limit of Sanya radar, thus causing the absence of corresponding non-specular echoes. Another possibility is that these optical meteors could appear at relatively low altitudes, for example below 80–90 km where plasma irregularities are difficult to be generated. By employing the Jicamarca radar observations during the two experiments on 12 July 2005 and 17 July 2007, Sugar et al. (2010) investigated the altitude distribution of non-specular echoes. Their results showed that the non-specular echoes rarely occurred at altitudes below 85 km, and 97% of the non-specular echo events occurred at 90–110 km. For the bright meteors appeared in the direction perpendicular to $\boldsymbol{B}$ (Figure 7), the possible cause responsible for the absence of non-specular echo could be that these meteors occurred at extremely low altitudes. This, however, needs to be investigated further and will be addressed in our future experiments of Sanya radar and double-station optical observations.

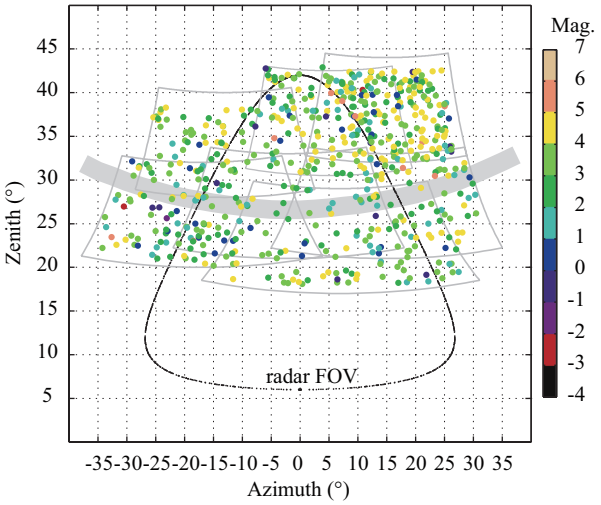


**Figure 7**. The angular locations of meteors detected by the optical system but not by the radar (a total of 608 meteors without simultaneous non-specular echos).

Based on the Sanya VHF radar, together with simultaneous double-station video observations, the following questions regarding non-specular echoes will be addressed in our future work: (1) Is there a clear cutoff altitude for the generation of meteor trail irregularities producing non-specular echoes? Though non-specular echoes have been detected by radars occasionally at relatively high and low altitudes, no definite cutoff altitude has so far been reported. Specifically, the features of meteoroids producing high/low altitude non-specular echoes remain unknown. In a recent experiment, we have found several cases of optical meteors and non-specular echoes simultaneously detected at high altitudes greater than 130 km. We are waiting for more cases (especially from the planned double-station video observations) to address this issue. (2) What is the relation between meteor mass and non-specular echo duration/intensity, which also depends on several other factors including background neutral wind and plasma density? (3) Is there a clear cutoff angle for the detection of non-specular echo while radar LOS points away from the direction perpendicular to geomagnetic field? The initial results from the simultaneous optical and radar observations presented in this study are consistent with earlier results from the limited statistical data of HPLA radars, which showed a cutoff angle of 12°. However, the MAARSY observations found several cases of non-specular echoes appearing in the direction nearly parallel to geomagnetic field (no cutoff angle). Simultaneous measurements by radar and double-station video systems that can provide information on the occurrence of meteors, and the accurate angular locations of corresponding non-specular echoes would be a good way to resolve this issue.

## 5. Conclusions

We have performed an experiment focusing on the simultaneous

optical meteor and radar non-specular echo observations at Sanya. The comparison of radar and optical measurements showed a good agreement between the angular positions of non-specular echoes and those of optical meteors, which verified the interferometry capability of Sanya radar for meteor trail irregularity observation. A general linear relationship was found to exist between the non-specular echo duration and its corresponding meteor visual magnitude. Further, the simultaneous radar and optical measurements showed some cases where optical meteors were detected but without simultaneous radar non-specular echoes. Possible factors leading to this phenomenon need to be investigated further. The accurate altitude of optical meteor would be required. This can be achieved by employing a double-station optical system planned to be installed in the near future.

## Acknowledgments

This study was carried out as a part of the project funded by the National Natural Science Foundation of China (41422404 and 41727803). The authors are grateful to the technical staff (Z. G. Huang, Z. Wu, J. L. Ji and W. Z. Chen) of Sanya observatory for their efforts for making the observations reported here, and to Dr. Nanan Balan for his efforts to improve the quality of this paper.

## References

Bourdillon, A., Haldoupis, C., Hanuise, C., Le Roux, Y., and Menard, J. (2005). Long duration meteor echoes characterized by Doppler spectrum bifurcation. *Geophys. Res. Lett.*, *32*, L05805. https://doi.org/10.1029/2004GL021685

Campbell-Brown, M. D., Kero, J., Szasz, C., Pellinen-Wannberg, A., and Weryk, R. J. (2012). Photometric and ionization masses of meteors with simultaneous EISCAT UHF radar and intensified video observations. *J. Geophys. Res.*, *117*, A09323. https://doi.org/10.1029/2012JA017800

Ceplecha, Z., Borovička, J., Elford, W. G., Revelle, D. O., Hawkes, R. L., Porubčan, V., and Šimek, M. (1998). Meteor phenomena and bodies. *Space Sci. Rev.*, *84*, 327–471. https://doi.org/10.1023/A:1005069928850

Chapin, E., and Kudeki, E. (1994). Radar interferometric imaging studies of long-duration meteor echoes observed at Jicamarca. *J. Geophys. Res.*, *99*, 8937–8949. https://doi.org/10.1029/93JA03198

Chau, J. L., Strelnikova, I., Schult, C., Oppenheim, M. M., Kelley, M. C., Stober, G., and Singer, W. (2014). Nonspecular meteor trails from non-field-aligned irregularities: Can they be explained by presence of charged meteor dust?. *Geophys. Res. Lett.*, *41*, 3336–3343. https://doi.org/10.1002/2014GL059922

Chu, Y. H., and Wang, C. Y. (2003). Interferometry observations of VHF backscatter from plasma irregularities induced by meteor in sporadic E region. *Geophys. Res. Lett.*, *30*(24), 2239. https://doi.org/10.1029/2003GL017703

Close, S., Hamlin, T., Oppenheim, M., Cox, L., and Colestock, P. (2008). Dependence of radar signal strength on frequency and aspect angle of nonspecular meteor trails. *J. Geophys. Res.*, *113*, A06203. https://doi.org/10.1029/2007JA012647

Dou, X.-K., Xue, X.-H., Li, T., Chen, T.-D., Chen, C., and Qiu, S.-C. (2010). Possible relations between meteors, enhanced electron density layers, and sporadic sodium layers. *J. Geophys. Res.*, *115*, A06311. https://doi.org/10.1029/2009JA014575

Dyrud, L. P., Kudeki, E., and Oppenheim, M. M. (2007). Modeling long duration meteor trails. *J. Geophys. Res.*, *112*, A12307. https://doi.org/10.1029/2007JA012692

Hawkes, R. L., Bussey, J. E., Macphee, S. L., Pollock, C. S., and Taggart, L. W. (2001). Techniques for high resolution meteor light curve investigations. In B. Warmbein, (Ed.), *Proceedings of the Meteoroids 2001 Conference* (pp. 281–286). Noordwijk: ESA Publications

Kelley, M. (2004). A new explanation for long-duration meteor radar echoes: Persistent charged dust trains. *Radio Sci.*, *39*, RS2015. https://doi.org/10.1029/2003RS002988

Kikwaya, J-B, Weryk, R. J., Campbell-Brown, M., and Brown, P.G. (2010). A model for saturation correction in meteor photometry. *Mon. Not. Roy. Astron. Soc.*, *404*, 387–398. https://doi.org/10.1111/j.1365-2966.2010.16294.x

Li, G. Z., Ning, B. Q., Patra, A. K., Wan, W. X., and Hu, L. (2011). Investigation of low-latitude E and valley region irregularities: Their relationship to equatorial plasma bubble bifurcation. *J. Geophys. Res.*, *116*, A11319. https://doi.org/10.1029/2011JA016895

Li, G. Z., Ning, B. Q., Hu, L. H., Chu, Y.-H., Reid, I. M., and Dolman, B. K. (2012). A comparison of lower thermospheric winds derived from range spread and specular meteor trail echoes. *J. Geophys. Res.*, *117*, A03310. https://doi.org/10.1029/2011JA016847

Li, G. Z., Ning, B. Q., Chu, Y.-H., Reid, I. M., Hu, L., Dolman, B. K., Xiong, J., Jiang, G., Yang, G., and Yan, C. (2014a). Structural evolution of long-duration meteor trail irregularities driven by neutral wind. *J. Geophys. Res. Space Phys.*, *119*, 10348–10357. https://doi.org/10.1002/2014JA020116

Li, G. Z., Ning, B. Q., and Hu, L. (2014b). Interferometry observations of low-latitude E-region irregularity patches using the Sanya VHF radar. *Sci. China Technol. Sci.*, *57*, 1552–1561. https://doi.org/10.1007/s11431-014-5592-3

Li, G. Z., Ning, B. Q., Wan, W. X., Reid, I. M., Hu, L. H., Yue, X. N., Younger, J. P., and Dolman, B. K. (2014c). Observational evidence of high-altitude meteor trail from radar interferometer. *Geophys. Res. Lett.*, *41*, 6583–6589. https://doi.org/10.1002/2014GL061478

Li, G. Z., Ning, B. Q., Liu, L. B., Abdu, M. A., Wan, W. X., and Hu, L. H. (2015). Shear in the zonal drifts of 3 m irregularities inside spread F plumes observed over Sanya. *J. Geophys. Res. Space Phys.*, *120*, 8146–8154. https://doi.org/10.1002/2015JA021497

Li, G. Z., Otsuka, Y., Ning, B. Q., Abdu, M. A., Yamamoto, M., Wan, W. X., Liu, L. B., and Abadi, P. (2016). Enhanced ionospheric plasma bubble generation in more active ITCZ. *Geophys. Res. Lett.*, *43*, 2389–2395. https://doi.org/10.1002/2016GL068145

Malhotra, A., Mathews, J. D., and Urbina, J. (2007). A radio science perspective on long-duration meteor trails. *J. Geophys. Res.*, *112*, A12303. https://doi.org/10.1029/2007JA012576

Maruyama, T., Kato, H., and Nakamura, M. (2008). Meteor-induced transient sporadic E as inferred from rapid-run ionosonde observations at midlatitudes. *J. Geophys. Res.*, *113*, A09308. https://doi.org/10.1029/2008JA013362

Mathews, J. D., Meisel, D. D., Hunter, K. P., Getman, V. S., and Zhou, Q. (1997). Very high resolution studies of micrometeors using the Arecibo 430 MHz radar. *Icarus*, *126*(1), 157–169. https://doi.org/10.1006/icar.1996.5641

Myers, J. R., Sande, C. B., Miller, A. C., Warren, W. H., and Tracewell, D. A. (2001). Sky 2000 Catalog v4. Goddard Space Flight Center, Ycat 5109.

Ning, B. Q., Hu, L. H., Li, G. Z., Liu, L. B., and Wan, W. X. (2012). The first time observations of low-latitude ionospheric irregularities by VHF radar in Hainan. *Sci. China Technol. Sci.*, *55*(5), 1189–1197. https://doi.org/10.1007/s11431-012-4800-2

Oppenheim, M. M., and Dimant, Y. (2006). Meteor induced ridge and trough formation and the structuring of the nighttime E-region ionosphere. *Geophys. Res. Lett.*, *33*, L24105. https://doi.org/10.1029/2006GL028267

Oppenheim, M. M., Sugar, G., Slowey, N. O., Bass, E., Chau, J. L., and Close, S. (2009). Remote sensing lower thermosphere wind profiles using non-specular meteor echoes. *Geophys. Res. Lett.*, *36*, L09817. https://doi.org/10.1029/2009GL037353

Oppenheim, M. M., and Dimant, Y. S. (2015). First 3-D simulations of meteor plasma dynamics and turbulence. *Geophys. Res. Lett.*, *42*, 681–687. https://doi.org/10.1002/2014GL062411

Reid, I. M. (2015). MF and HF radar techniques for investigating the dynamics and structure of the 50 to 110 km height region: a review. *Progress Earth Planetary Sci.*. https://doi.org/10.1186/s40645-015-0060-7

Sugar, G., Oppenheim, M. M., Bass, E., and Chau, J. L. (2010). Nonspecular meteor trail altitude distributions and durations observed by a 50 MHz high-power radar. *J. Geophys. Res.*, *115*, A12334. https://doi.org/10.1029/2010JA015705

Zhou, Q. H., Mathews, J. D., and Nakamura, T. (2001). Implications of meteor observations by the mu radar. *Geophys. Res. Lett.*, *28*, 1399–1402. https://doi.org/10.1029/2000GL012504